Available online at www.sciencedirect.com

ScienceDirect

Ceramics International 40 (2014) 675–681

CERAMICS INTERNATIONAL

www.elsevier.com/locate/ceramint

Magnetic dilution effect of nano-crystalline $NiFe_2O_4$ synthesized via sucrose-assisted combustion route

M.A. Gabal*[,1], S. Kosa, T.S. El Muttairi

Chemistry Department, Faculty of Science, King Abdulaziz University, Jeddah, Saudi Arabia

Received 5 May 2013; received in revised form 25 May 2013; accepted 15 June 2013
Available online 21 June 2013

Abstract

Sucrose assisted combustion route was utilized to synthesize nano-crystalline Cr-substituted nickel ferrites, $NiFe_{2-x}Cr_xO_4$ ($x=0.0$–1.0). The synthesized samples were characterized by X-ray diffraction (XRD), Fourier transform infrared (FT-IR), transmission electron microscopy (TEM) and vibrating sample magnetometer (VSM) techniques to investigate the effect of Cr-substitution on the structural and magnetic properties of the entire system. Single-phase formation was checked using XRD and a proper cation distribution was estimated depending on the related structural parameters. FT-IR absorption bands were found to be in the expected range, which fortifies the spinel formation. The change in the structural properties by the addition of Cr^{3+} ions was discussed from the view point of ionic radii of the entire ions. TEM revealed the agglomeration nature of the synthesized powders. The magnetic properties were strongly affected by Cr-substitution. The decrease in the saturation magnetization and coercivity with increasing Cr-content was attributed to magnetic moments and magneto-crystalline anisotropy of the entire ions, respectively.

Keywords: $NiFe_2O_4$; Cation distribution; Magnetization; Sucrose

1. Introduction

Due to their high electrical resistivity, low magnetic coercivity, low eddy current losses, high Curie temperature, mechanical hardness, chemical stability and reasonable cost, polycrystalline ferrites are preferred for many technological applications such as high-quality filters, sensors, satellite communications, computer components, memory devices, antenna rods, radio frequency circuits, transformer cores, etc. [1,2].

The crystal structure of these materials controls their magnetic, electrical, and physical properties and can be in turn influenced by their preparation methodology. In the literature, numerous wet-chemical methods were successfully used for synthesis of nano-sized ferrites [3–9]. Among these methods, the combustion route is found to be the fastest, simplest, most cost effective and less energy consuming for synthesis of homogeneous, nano-crystalline and chemically pure products without high temperature calcining stages [10,11].

The interesting electrical and magnetic properties of these ferrites can be tailored by controlling different types and amounts of substituents. Several researchers have studied the effect of Cr-substitution on different properties of ferrites [12–17]. Patange et al. [18] prepared $NiFe_{2-x}Cr_xO_4$ ($x=0.0$–1.0) by co-precipitation method. X-ray diffraction (XRD) showed cubic spinel structures with unit cell dimensions decrease for increasing Cr^{3+} content.

Patange et al. [19] prepared ultrafine Cr-substituted nickel ferrite by co-precipitation method using sulfates. The estimated cation distribution using XRD indicates that Cr occupy octahedral sites. The saturation magnetization, Curie temperature and magneton number decrease with increasing Cr-content.

Gabal and Al Angari [17] prepared polycrystalline $NiFe_{2-x}Cr_xO_4$ ($0\leq x\leq 1$) through oxalate impregnation method. The samples were characterized by XRD, Fourier transform infrared (FT-IR), AC-conductivity, vibrating sample magnetometer (VSM) and magnetic susceptibility measurements. Lattice constant slightly decreases with increasing Cr-content.

*Corresponding author. Tel.: +966 557071572.
E-mail address: mgabalabdonada@yahoo.com (M.A. Gabal).
[1]Permanent address: Chemistry Department, Faculty of Science, Benha University, Benha, Egypt.

0272-8842/$ - see front matter © 2013 Elsevier Ltd and Techna Group S.r.l. All rights reserved.
http://dx.doi.org/10.1016/j.ceramint.2013.06.054

Singhal and Chandra [20] investigated cation distribution in Cr-substituted nickel ferrites, prepared by aerosol route, using XRD, VSM and Mossbauer studies. It was found that Cr occupies octahedral sites up to $x=0.8$, and then enters into tetrahedral sites.

Singh et al. [15] synthesized $NiFe_{2-x}Cr_xO_4$ ($0\leq x\leq 1$) by a precipitation method. Their structural properties have been investigated using IR, XRD and BET surface area measurements.

Using XRD and Mössbauer spectroscopic techniques, Gismelseed and Yousif [21] revealed that the cation distributions of $NiFe_{2-x}Cr_xO_4$ ($x=0.0$–1.4) are gradually transferred from perfect inverse spinel to partially normal one. The same observation was also reported by Lee et al. [22] using magnetic measurements and Mössbauer spectroscopy.

In the present study, we will adopt two strategies for modifying the properties of $NiFe_{2-x}Cr_xO_4$ ($x=0.0$–1.0) ferrites; the first is to develop a new preparation method and the second is to study the effect of partial replacement of iron by magnetically weak chromium ions on the structural and magnetic properties. In this context, the entire ferrites will be prepared via sucrose-assisted combustion method [10,11]. The structural and magnetic properties will be characterized using XRD, FT-IR, TEM and VSM techniques.

2. Materials and methods

$NiFe_{2-x}Cr_xO_4$ ferrites ($x=0.0$–1.0) were prepared via sucrose auto-combustion method. In this process, the easily oxidized metal nitrates acting as an oxidant are mixed with sucrose, which acts as a reductant. The redox reaction is initiated using heat generated from hot plate stirrer until the self-combustion exothermic reaction is propagated.

Stoichiometric ratios of the respective metal nitrates were dissolved in 100 ml distilled water and the appropriate amount of sucrose aqueous solution was mixed thoroughly. The resulting solution was kept at 60 °C for 30 min under vigorous stirring. Ammonia solution (50%, v/v) was then added dropwise up to pH of 7. At this point, a sticky gel was obtained which converted to a solid sticky gel by evaporation, at 100 °C. Once solid gel is obtained, the temperature of the hot plate is raised to the maximum to give a chance for gel combustion process to occur. The violence combustion, accompanied by the evolution of large quantities of gases, resulted in the formation of carbonaceous black colored fluffy mass. The loose powder obtained after complete combustion was then ground and stored in a dessicator. This powder is then called as-prepared sucrose precursor.

Thermal decomposition behavior of the gel-precursor was characterized using simultaneous differential thermal analysis–thermogravimetry (DTA-TG) techniques. The experiment was measured in air using a Perkin-Elmer thermal analyzer up to 600 °C at a heating rate of 5 °C min^{-1}.

The crystal structure of the as-prepared samples was characterized by a Bruker D8 Advance X-ray diffractometer using CuKα radiation ($\lambda=0.154$ nm). The patterns were recorded in the 2θ range of 10–80° at scanning rate 1°/min.

FT-IR spectra were recorded on a Shimadzu FT-IR 8400 spectrophotometer using KBr pellet technique.

The morphology of the powder was revealed using a JEOL 2010 TEM operating at an accelerating voltage of 100 kV. The sample was prepared by dropping the ethanol dispersion on a carbon-coated copper grid.

Magnetic measurements were performed using a vibrational sample magnetometer (VSM-9600 M) at room temperature with maximum applied magnetic field of 5 kOe.

3. Results and discussion

3.1. Complexation mechanism and ferrite formation

The combustion route is based on the mixing of metal nitrates oxidizing agents and an organic fuel, acting as a reducing agent. In this case, external heat is needed to initiate the ignition resulting in self-sustainment of an exothermic redox reaction. The combustion processes are mainly dependent on the nature of the fuel. Farhadi and Zaidi [11] used various organic fuels such as urea, citric acid, glycine and sucrose for the preparation of $BiFeO_3$. Among them, sucrose was found to be the best one resulting in the formation of pure and nano-size ferrite.

Sucrose with the molecular formula $C_{12}H_{22}O_{11}$ is a disaccharide composed of glucose and fructose monosaccharides linked via an ether bond. This bond, formed between the reducing ends of both glucose and fructose, is called a glycosidic linkage [23]. Under the present experimental conditions, sucrose can function as both complexing agent and fuel. During evaporation, in the presence of metal nitrates oxidants, the sucrose was hydrolyzed (in the presence of H^+ from nitric acid) to glucose and fructose, which can be further oxidized into saccharic acid, glycolic acid and trihydroxybutyric acid with a number of −COOH and −OH groups [11,24]. The process is then quite similar to the citric acid complexation mechanism in which −COOH groups can be easily combined with metal ions.

The pH of metals citrate complex solution was adjusted to about 7 by adding ammonium hydroxide in order to promote the polysterification reaction and formation of viscous resin complex [25].

During heating at 60 °C, the water was evaporated and the constituents of the solution were polymerized until the solution became a black sticky gel. At 100 °C, this gel solidified and on further rising temperature, a point of spontaneous combustion was reached at which the organic constituents were decomposed with the generation of a mass of gases such as CO_2, N_2 and H_2O [11]. These gases make the sticky gel to expand more than 10 times, resulting in the formation of a highly porous ferrites network. The combustion is finished in a very short time so that no grains can occur and very fine particles only can be obtained. The typical total combustion reaction can be written as follows:

$$Ni(NO_3)_2.6H_2O+2Fe(NO_3)_3.9H_2O+C_{12}H_{22}O_{11}+2O_2 \rightarrow NiFe_2O_4+12CO_2+4N_2+35H_2O$$

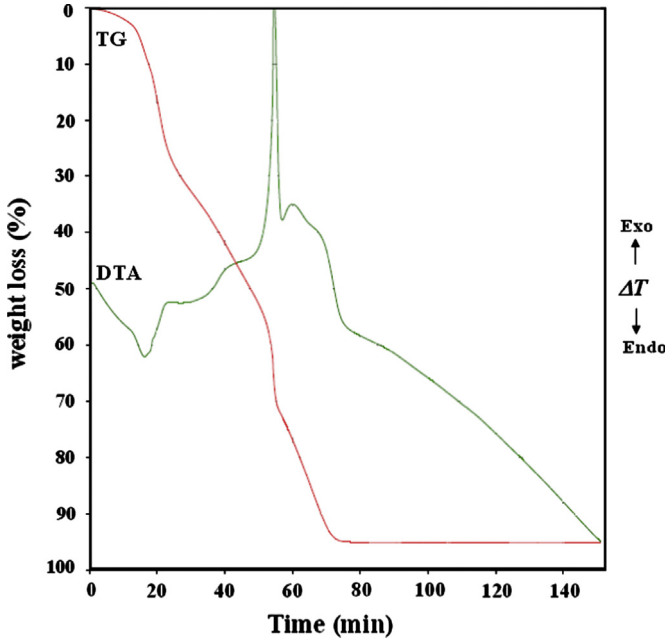

Fig. 1. DTA–TG curves in air of gel-precursor with $x=0.0$. Heating rate = 5 °C min^{-1}.

3.2. Thermal decomposition behavior of gel-precursor

Fig. 1 shows DTA–TG curves of sucrose gel-precursor with $x=0$. From the figure it is clear that only three-weight loss processes are occurring in the temperature range 30–405 °C. The first weight loss step can be assigned to the evaporation of water and it is evidenced by a broad endothermic DTA peak at 120 °C. The second step is accompanied by two exothermic DTA peaks (broad: 220–310 °C and sharp: 347 °C) while the third one is characterized by only one weak exothermic DTA peak. These two exothermic nature processes can be attributed to the auto-combustion reaction between nitrates and sucrose organic moiety. Almost no weight loss occurred over 405 °C indicating the completion of the gel thermal decomposition.

3.3. X-ray diffraction analysis

Structure of the as-prepared precursors was characterized using XRD technique. X-ray diffractograms (Fig. 2) showed the formation of single-phase cubic spinel. The peaks can be indexed to (111), (220), (311), (222), (400), (422), (511) and (440) planes. The broadness of the diffraction peaks suggests the nano-sized nature of the prepared powders. The average crystallite sizes were calculated using the Debye–Scherrer formula [26] and are reported in Table 1. The obvious decrease in the average crystallite size with increasing Cr-content can be attributed to inhibition of the grain boundary mobility, responsible for grain growth, by the successive addition of chromium. Similar results for Cr-substituted ferrites were reported in the literature [26,27].

The patterns also show a very slight shift in the peaks position, towards lower *d*-spacing values, with increasing Cr-content. The experimental lattice parameters (a_{exp}) [26] exhibited a gradual decrease with increasing Cr-content (Table 1). This behavior followed Vegard's law [28] and can be explained on the basis of the difference between ionic radii of the substituted ions (Fe^{3+}: 0.645 Å and Cr^{3+}: 0.63 Å) [29]. The calculated X-ray density (*Dx*) [26] is obviously constant at all compositions (Table 1). The gradual decrease in the molecular weight of the sample, due to Cr-substitution, is accompanied by a decrease in the lattice constant.

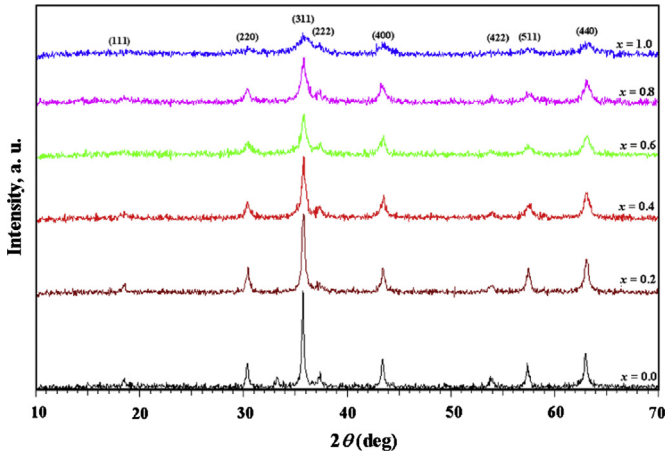

Fig. 2. XRD patterns of the as-prepared precursors.

$NiFe_2O_4$ is a well-known inverse spinel and the gradual substitution with Cr^{3+} ions will result in the subsequent replacement of Fe^{3+} ions located in its octahedral sites [30]. According to this expectation, the cation distribution of the entire system can be suggested as $(Fe^{3+})[Ni^{2+}Fe^{3+}_{1-x}Cr_x]O^{2-}_4$. The theoretical lattice parameters (a_{th}) calculated according to this distribution (Table 1) agree well with those experimentally obtained, which suggests proper cation distribution. The number of iron atoms located in the tetrahedral site, i.e. the inversion factor (γ), is constant and equals unity.

The radii of the tetrahedral (r_A) and octahedral sites (r_B), oxygen positional parameter (u), hopping length of A-sites (L_A) and B-sites (L_B) and intercationic distances were calculated [26] and are reported in Table 1. The constant oxygen positional parameter suggests constant tetrahedral cation distribution and preferential occupancy of Cr^{3+} ions by octahedral sites for all the samples. The other reported values could be discussed according to the radius of Ni^{2+}, Cr^{3+} and Fe^{3+} ions and their cation distribution.

3.4. FT-IR spectroscopy

FT-IR spectra of the as-prepared precursors (Fig. 3) reveal the presence of two strong absorption bands υ_1 and υ_2 which lie in the expected range of cubic spinel-type ferrites [31]: the high-frequency band υ_1 belongs to the tetrahedral site while the low-frequency band υ_2 to the octahedral complexes. The change in the band position with Cr-content is indicated in Table 2. It can be seen that the value of υ_1 is almost constant while that of υ_2 slightly increases with increasing chromium. This observation indicates the preferential occupancy of Cr^{3+} ions by the octahedral sites of the entire system.

Table 1
Structural data of $NiFe_{2-x}Cr_xO_4$ system.

Cation distribution (x)	a, (Å)		r (Å)		L (nm)	D_X (g cm^{-3})	γ	u (Å)	L_A (Å)	L_B (Å)	Tet. bond	Oct. bond	Tet. edge	Oct. edge (Å)	
	a_{exp}	a_{th}	r_A	r_B										Shared	Unshared
(Fe)[NiFe]O_4	8.3359	8.3391	0.49	0.668	34	5.37	1.0	0.379	3.61	2.95	1.869	2.047	3.053	2.841	2.948
(Fe)[$NiFe_{0.8}Cr_{0.2}$]O_4	8.3292	8.3310	0.49	0.665	22	5.37	1.0	0.379	3.61	2.94	1.869	2.045	3.053	2.836	2.946
(Fe)[$NiFe_{0.6}Cr_{0.4}$]O_4	8.3213	8.3230	0.49	0.662	16	5.37	1.0	0.379	3.60	2.94	1.869	2.042	3.053	2.830	2.943
(Fe)[$NiFe_{0.4}Cr_{0.6}$]O_4	8.3204	8.3150	0.49	0.659	14	5.35	1.0	0.379	3.60	2.94	1.869	2.041	3.053	2.829	2.943
(Fe)[$NiFe_{0.2}Cr_{0.8}$]O_4	8.3198	8.3089	0.49	0.656	12	5.33	1.0	0.379	3.61	2.94	1.869	2.045	3.053	2.837	2.947
($Fe_{0.8}Cr_{0.2}$)[$NiFe_{0.2}Cr_{0.8}$]O_4	8.3098	8.2990	0.49	0.652	9	5.34	1.0	0.379	3.60	2.93	1.869	2.037	3.053	2.822	2.939

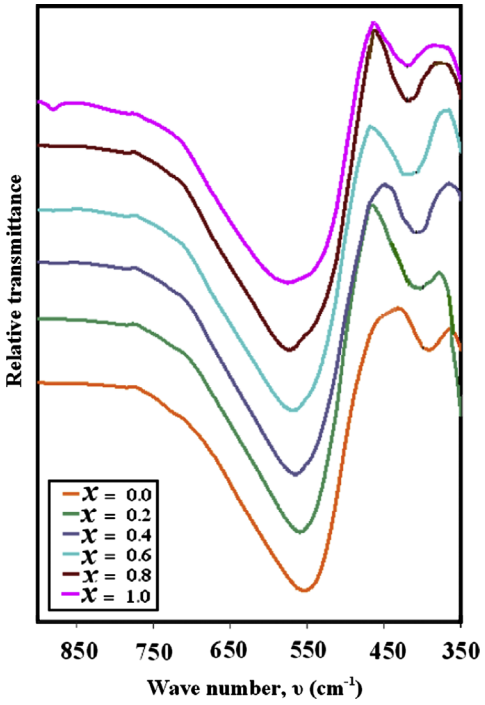

Fig. 3. FT-IR spectra of $NiFe_{2-x}Cr_xO_4$ system.

This substitution will result in the shortening of Fe^{3+}–O^{2-} bond due to replacement of the larger Fe^{3+} ions by the smaller Cr^{3+} ions and therefore increasing frequency.

The observed behavior in the band's positions with increasing Cr-content agrees well with the calculated radius of the tetrahedral and octahedral sites reported in Table 2, which again suggests proper and consistent cation distribution.

The force constants of tetrahedral site (k_t) and octahedral site (k_o), calculated according to Waldron [31], are reported in Table 2. The Cr-substitution successively replaces octahedral Fe^{3+} ions and consequently increases the octahedral force constant. On the other hand, the tetrahedral force constant remains hardly unchanged.

3.5. TEM

Typical TEM images of the entire ferrite system are presented in Fig. 4. The samples with $x=0.2$ and 0.8 exhibit spherical nano-sized particles agglomerated in cluster-type shape. The observed sizes agree well with those obtained from XRD measurements. This agglomeration can be attributed to magnetostatic interaction between particles [32] or for a permanent magnetic moment experienced by the nanoparticles proportional to their volume [26].

3.6. Magnetic studies

Magnetic hysteresis loops for the entire $NiFe_{2-x}Cr_xO_4$ system are shown in Fig. 5. From the figure, it is clear that all the samples exhibit a clear hysteresis behavior under applied magnetic field at room temperature. The saturation magnetization (M_s), coercivity (H_c), magnetic moment (η_B) in

Table 2
FT-IR spectral data and magnetic parameters of $NiFe_{2-x}Cr_xO_4$ system.

x	ν_1 (cm^{-1})	ν_2 (cm^{-1})	k_t	K_o	Hysteresis loop				$\eta_B(x)$
					M_s	M_r	H_c	η_B	
0.0	561	396	1.34	0.95	34.5	10.3	199	1.44	2.0
0.2	562	398	1.34	0.96	28.0	6.0	148	1.17	1.6
0.4	566	407	1.37	1.00	18.8	2.8	105	0.78	1.2
0.6	570	400	1.38	0.95	9.8	1.1	80	0.41	0.8
0.8	569	408	1.38	0.99	8.1	1.4	172	0.33	0.4
1.0	564	412	1.34	1.00	2.6	0.1	136	0.11	0.0

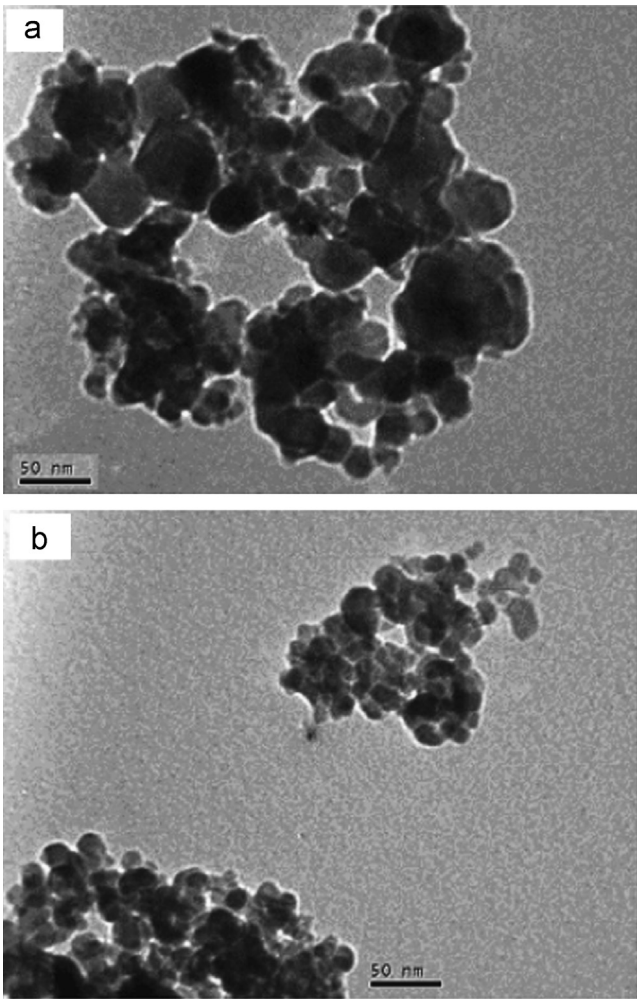

Fig. 4. TEM images of $NiFe_{2-x}Cr_xO_4$ system: (a) $x=0.2$ and (b) $x=0.8$. Scale bar: 50 nm.

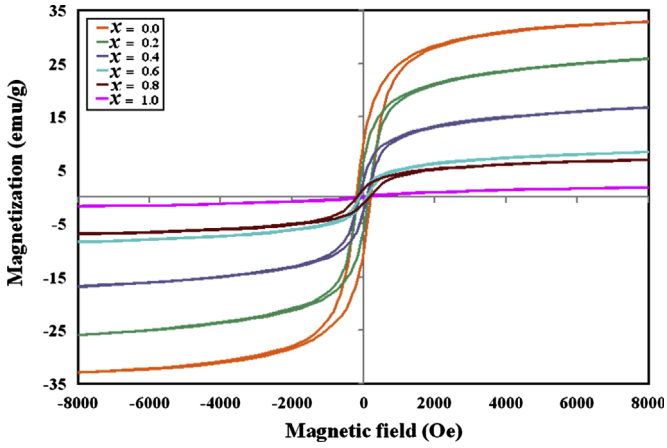

Fig. 5. Magnetic hysteresis loops for $NiFe_{2-x}Cr_xO_4$ system.

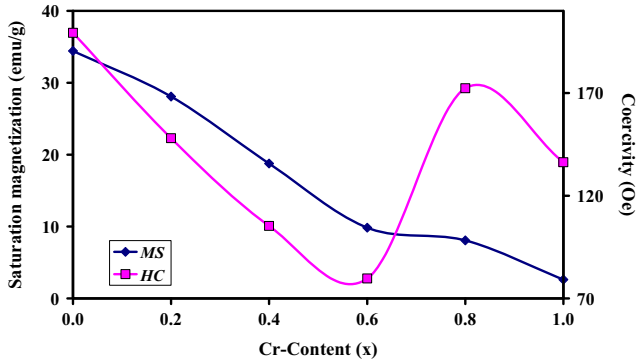

Fig. 6. Variation of the saturation magnetization and coercivity with x in $NiFe_{2-x}Cr_xO_4$ system.

Bohr magneton and remanent magnetization (M_r) are presented in Table 2. Fig. 6 exhibits the change in the saturation magnetization (M_s) and coercivity (H_c) with chromium content.

According to Neel's two-sublattice model of ferrimagnetism [33], taking into consideration the estimated cation distribution and using ionic magnetic moments of Fe^{3+}, Cr^{3+} and Ni^{2+} (5 μ_B, 3 μ_B and 2 μ_B, respectively), the rapid decrease in magnetization values with increasing Cr-content can be attributed to the dilution of B-sublattice magnetization by addition of Cr^{3+} ions. On substitution, Cr^{3+} ions preferably occupy B-sites and thus replace the Fe^{3+} ions. Due to the larger magnetic moment of Fe^{3+} ions as compared to that of Cr^{3+} ions, as the number of Fe^{3+} ions decreases, the magnetization of B-sublattice consequently decreases, resulting in the observed decrease in the saturation magnetization.

The obvious difference between the observed magnetic moment (calculated using saturation magnetization), η_B and the theoretical Neel's magnetic moment $\eta_B(x)$ (Table 2) suggested non-colinear spin ordering [34]. In addition, the magnetization values obtained under the present experimental

conditions are found to be smaller than those reported in the literature for Cr-substituted nickel ferrites prepared via other methods [9,20,34,35].

The coercivity is influenced by many factors such as magnetocrystallinity, microstrain, magnetic particle morphology, size distribution, anisotropy, and magnetic domain size. The general trend of the coercivity of the present system is to decrease with increasing Cr-content with an obvious increase at x=0.8.

The decrease in the coercivity values with increasing Cr-content can be attributed in this system to the decrease in magnetocrystalline anisotropy (K_1). Compared with larger magnetocrystalline anisotropy for $NiFe_2O_4$ ferrite, chromium ferrite has negative magnetocrystalline anisotropy [32]. Thus, the summation of the individual anisotropies will decrease by the addition of Cr and hence decreases coercivity. Furthermore, the lower values of the coercive field indicate that the entire materials are soft ferromagnetic, which enhances their uses in high-frequency transformers applications.

4. Conclusions

Single-phase Cr-substituted nickel ferrites nanopowders were successfully prepared by sucrose assisted auto-combustion method. The cation distribution was estimated using XRD and was fortified using FT-IR and VSM measurements. All the measured structural and magnetic parameters showed an obvious decrease with increasing Cr-content. The magnetizations of entire samples are lower than those reported in the literature. The low coercivity values obtained enhance their uses in high- frequency transformers applications.

Acknowledgment

The authors are grateful to Deanship of Scientific Research (DSR), King Abdulaziz University, Jeddah, for providing financial support for this work. Also, the authors would like to express their thanks to Dr. Sharief, Chemistry Department, Benha University, for his help and cooperation.

References

[1] R. Valenzuela, Magnetic Ceramics, Cambridge University Press, Cambridge, 1994.
[2] A. Goldman, Handbook of Modern Ferromagnetic Materials, Kluwer Academic Publishers, Boston, USA, 1999.
[3] W. Lv, B. Liua, Z. Luoa, X. Rena, P. Zhang, XRD studies on the nanosized copper ferrite powders synthesized by sonochemical method, Journal of Alloys. and Compounds 465 (2008) 261–264.
[4] V.D. Kapse, S.A. Ghosh, F.C. Raghuwanshi, S.D. Kapse, Nanocrystalline spinel $Ni_{0.6}Zn_{0.4}Fe_2O_4$: a novel material for H_2S sensing, Materials Chemistry and Physics 113 (2009) 638–644.
[5] S. Thakur, S.C. Katyal, M. Singh, Structural and magnetic properties of nano nickel–zinc ferrite synthesized by reverse micelle technique, Journal of Magnetism and Magnetic Materials 321 (2009) 1–7.
[6] M. Gu, B. Yue, R. Bao, H. He, Template synthesis of magnetic one-dimensional nanostructured spinel MFe_2O_4 (M=Ni, Mg, Co), Materials Research Bulletin 44 (2009) 1422–1427.
[7] Y. Fu, D. Hung, C. Cheng, F. Tsai, Y. Yao, Non-isothermal crystallization kinetics and microwave properties of $Bi_{0.75}Y_{2.25}Fe_5O_{12}$ prepared by co-precipitation, Ceramics International 35 (2009) 559–564.
[8] P.P. Hankare, U.B. Sankpal, R.P. Patil, I.S. Mulla, P.D. Lokhande, N.S. Gajbhiye, Synthesis and characterization of $CoCr_xFe_{2-x}O_4$ nanoparticles, Journal of Alloys and Compounds 485 (2009) 798–801.
[9] M.A. Gabal, Y.M. Al-Angari, Effect of diamagnetic substitution on the structural, magnetic and electrical properties of $NiFe_2O_4$, Materials Chemistry and Physics 115 (2009) 578–584.
[10] S.S. Kamble, V.S. Jagtap, P.C. Pingale, Synthesis of $Mg_{0.48}Cu_{0.12}Zn_{0.40}Fe_2O_4$ ferrite and its aptness for multilayer chip component application, Ceramics International 39 (2013) 3597–3601.
[11] S. Farhadi, M. Zaidi, Bismuth ferrite ($BiFeO_3$) nanopowder prepared by sucrose-assisted combustion method: a novel and reusable heterogeneous catalyst for acetylation of amines, alcohols and phenols under solvent-free conditions, Journal of Molecular Catalysis A: Chemical 299 (2009) 18–25.
[12] K.P. Chae, Y.B. Lee, J.G. Lee, S.H. Lee, Crystallographic and magnetic properties of $CoCr_xFe_{2-x}O_4$ ferrite powders, Journal of Magnetism and Magnetic Materials 220 (2000) 59–64.
[13] D.R. Mane, U.N. Devatwal, K.M. Jadhav, Structural and magnetic properties of aluminium and chromium co-substituted cobalt ferrite, Materials Letters 44 (2000) 91–95.
[14] S.J. Lee, C.C. Lo, P.N. Matlage, S.H. Song, Y. Melikhov, J.E. Snyder, D.C. Jiles, Magnetic and magnetoelastic properties of Cr-substituted cobalt ferrite, Journal of Applied Physics 102 (2007) 073910–073913.
[15] R.N. Singh, J.P. Singh, B. Lal, M.J.K. Thomas, S. Bera, New $NiFe_{2-x}Cr_xO_4$ spinel films for O_2 evolution in alkaline solutions, Electrochimica Acta 51 (2006) 5515–5523.
[16] D. Ravinder, K.S. Reddy, P. Mahesh, T.B. Rao, Y.C. Venudhar, Electrical conductivity of chromium substituted copper ferrites, Journal of Alloys and Compounds 370 (2004) L17–L22.
[17] M.A. Gabal, Structural and magnetic properties of nano-sized Cu–Cr ferrites prepared through a simple method using egg white, Materials Letters 64 (2010) 1887–1890.
[18] S.M. Patange, S.E. Shirsath, S.S. Jadhav, K.S. Lohar, D.R. Mane, K.M. Jadhav, Rietveld refinement and switching properties of Cr^{3+} substituted $NiFe_2O_4$ ferrites, Materials Letters 64 (2010) 722–724.
[19] S. Patange, S. Shirsath, B. Toksha, S. Jadhav, S. Shukla, K. Jadhav, Cation distribution by Rietveld, spectral and magnetic studies of chromium-substituted nickel ferrites, Applied Physics A: Materials Science and Processing 95 (2009) 429–434.
[20] S. Singhal, K. Chandra, Cation distribution and magnetic properties in chromium-substituted nickel ferrites prepared using aerosol route, Journal of Solid State Chemistry 180 (2007) 296–300.
[21] A.M. Gismelseed, A.A. Yousif, Mössbauer study of chromium-substituted nickel ferrites, Physica B: Condensed Matter 370 (2005) 215–222.
[22] S.H. Lee, S.J. Yoon, G.J. Lee, H.S. Kim, C.H. Yo, K. Ahn, D.H. Lee, K.H. Kim, Electrical and magnetic properties of $NiCr_xFe_{2-x}O_4$ spinel ($0 \le x \le 0.6$), Materials Chemistry and Physics 61 (1999) 147–152.
[23] C.A. Beevers, T.R.R. Mc Donald, J.H. Robertson, F. Stern, The crystal structure of sucrose, Acta Crystallographica 5 (1952) 689–690.
[24] E.A. Souza, J.G.S. Duque, L. Kubota, C.T. Meneses, Synthesis and characterization of NiO and $NiFe_2O_4$ nanoparticles obtained by a sucrose-based route, Journal of Physics and Chemistry of Solids 68 (2007) 594–599.
[25] R. Gimenes, M.R. Baldissera, M.R.A. da Silva, C.A. da Silveira, D.A. W. Soares, L.A. Perazolli, M.R. da Silva, M.A. Zaghete, Structural and magnetic characterization of $Mn_xZn_{1-x}Fe_2O_4$ (x=0.2; 0.35; 0.65; 0.8; 1.0) ferrites obtained by the citrate precursor method, Ceramics International 38 (2012) 741–746.
[26] M.A. Gabal, R.M. El-Shishtawy, Y.M. Al Angari, Structural and magnetic properties of nano-crystalline Ni–Zn ferrites synthesized using egg-white precursor, Journal of Magnetism and Magnetic Materials 324 (2012) 2258–2264.
[27] R.K. Sharma, O. Suwalka, N. Lakshmi, K. Venugopalan, A. Banerjee, P.A. Joy, Synthesis of chromium substituted nano particles of cobalt zinc ferrites by co-precipitation, Materials Letters 59 (2005) 3402.

[28] C.G. Whinfrey, D.W. Eckort, A. Tayber, Preparation and X-ray diffraction data[1] for dome rare earth stannates, Journal of the American Chemical Society 82 (1960) 2695–2697.
[29] R.D. Shannon, Revised effective ionic radii and systematic studies of interatomic distances in halides and chalcogenides, Acta Crystallographica: A 32 (1976) 751–767.
[30] A. Goldman, Modern Ferrite Technology, Marcel Dekker, Inc., New York, 1993.
[31] R.D. Waldron, Infrared Spectra of Ferrites, Physical Review 99 (1955) 1727–1735.
[32] S.T. Alone, Sagar E. Shirsath, R.H. Kadam, K.M. Jadhav, Chemical synthesis, structural and magnetic properties of nano-structured Co–Zn–Fe–Cr ferrite, Journal of Alloys and Compounds 509 (2011) 5055–5060.
[33] L. Neel, C.R. Acad, Sciences Paris 230 (1950) 375.
[34] S.M. Patange, S.E. Shirsath, B.G. Toksha, S.S. Jadhav, K.M. Jadhav, Electrical and magnetic properties of Cr^{3+} substituted nanocrystalline nickel ferrite, Journal of Applied Physics 106 (2009) 023914.
[35] S.H. Lee, S.J. Yoon, G.J. Lee, H.S. Kim, C.H. Yo, K. Ahn, D.H. Lee, K. H. Kim, Electrical and magnetic properties of $NiCr_xFe_{2-x}O_4$ spinel ($0 \leq x \leq 0.6$), Materials Chemistry and Physics 61 (1999) 147.